Planarised optical fiber composite using flame hydrolysis deposition demonstrating an integrated FBG anemometer

Christopher Holmes,* James C. Gates and Peter G. R. Smith

Optoelectronics Research Centre, University of Southampton, Southampton, SO17 1BJ, UK
chh@orc.soton.ac.uk

Abstract: This paper reports for the first time a planarised optical fiber composite formed using Flame Hydrolysis Deposition (FHD). As a way of format demonstration a Micro-Opto-Electro-Mechanical (MOEMS) hot wire anemometer is formed using micro-fabrication processing. The planarised device is rigidly secured to a silicon wafer using optical quality doped silica that has been deposited using flame hydrolysis and consolidated at high temperature. The resulting structure can withstand temperatures exceeding 580K and is sensitive enough to resolve free and forced convection interactions at low fluid velocity.

OCIS codes: (120.0120) Instrumentation, measurement, and metrology; (060.2370) Fiber optics sensors; (060.3735) Fiber Bragg gratings; (130.3990) Micro-optical devices.

References and links

1. G. Roelkens, D. Vermeulen, S. Selvaraja, R. Halir, W. Bogaerts, and D. Van Thourhout, "Grating-Based Optical Fiber Interfaces for Silicon-on-Insulator Photonic Integrated Circuits," IEEE J. Quantum Electron. **17**(3), 571–580 (2011).
2. C. Kopp, B. Ben Bakir, J. Fedeli, R. Orobtchouk, F. Schrank, H. Porte, L. Zimmermann, and T. Tekin, "Silicon Photonic Circuits : On-CMOS Integration, Fiber Optical Coupling, and Packaging," IEEE J. Sel. Top. Quantum Electron. **17**(3), 498–509 (2011).
3. J. P. Koplow, S. W. Moore, and D. A. V. Kliner, "A new method for side pumping of double-clad fiber sources," IEEE J. Quantum Electron. **39**(4), 529–540 (2003).
4. D. J. Ripin and L. Goldberg, "High efficiency side-coupling of light into optical fibres using imbedded v-grooves," Electron. Lett. **31**(25), 2204–2205 (1995).
5. Y. Tian, W. Wang, N. Wu, X. Zou, C. Guthy, and X. Wang, "A miniature fiber optic refractive index sensor built in a MEMS-based microchannel," Sensors (Basel) **11**(12), 1078–1087 (2011).
6. C. Pang, H. Bae, A. Gupta, K. Bryden, and M. Yu, "MEMS Fabry-Perot sensor interrogated by optical system-on-a-chip for simultaneous pressure and temperature sensing," Opt. Express **21**(19), 21829–21839 (2013).
7. V. P. Wnuk, A. Méndez, C. Ave, S. Ferguson, and T. Graver, "Process for Mounting and Packaging of Fiber Bragg Grating Strain Sensors for use in Harsh Environment Applications," Smart Struct. Conf. **46**, (2005).
8. A. Saran, D. C. Abeysinghe, R. Flenniken, and J. T. Boyd, "Anodic bonding of optical fibers-to-silicon for integrating MEMS devices and optical fibers," J. Micromech. Microeng. **13**(2), 346–351 (2003).
9. R. Knechtel, "Glass frit bonding: an universal technology for wafer level encapsulation and packaging," Microsyst. Technol. **12**(1-2), 63–68 (2005).
10. A. D. Yablon, *Optical Fiber Fusion Splicing*, Springer Series in Optical Sciences (Springer, 2005).
11. M. Kawachi, "Silica waveguides on silicon and their application to integrated-optic components," Opt. Quantum Electron. **22**(5), 391–416 (1990).
12. H. L. Rogers, S. Ambran, C. Holmes, P. G. R. Smith, and J. C. Gates, "In situ loss measurement of direct UV-written waveguides using integrated Bragg gratings," Opt. Lett. **35**(17), 2849–2851 (2010).
13. A. Kilian, J. Kirchhof, B. Kuhlow, G. Przyrembel, and W. Wischmann, "Birefringence Free Planar Optical Waveguide Made by Flame Hydrolysis Deposition (FHD) Through Tailoring of the Overcladding," J. Lightwave Technol. **18**(2), 193–198 (2000).
14. P. Dumais, "Thermal Stress Birefringence in Buried-Core Waveguides with Over-Etch," IEEE J. Quantum Electron. **47**(7), 989–996 (2011).
15. J. Salort, A. Monfardini, and P.-E. Roche, "Cantilever anemometer based on a superconducting micro-resonator: application to superfluid turbulence," Rev. Sci. Instrum. **83**(12), 125002 (2012).
16. P. Zyłka, P. Modrzynski, and P. Janus, "Vortex Anemometer Using MEMS Cantilever Sensor," J. Micromechanical Syst. **19**(6), 1485–1489 (2010).

#224955 - $15.00 USD Received 15 Oct 2014; revised 27 Nov 2014; accepted 9 Dec 2014; published 19 Dec 2014

17. M. Schwerter, T. Beutel, M. Leester-Schädel, S. Büttgenbach, and A. Dietzel, "Flexible hot-film anemometer arrays on curved structures for active flow control on airplane wings," Microsyst. Technol. **20**(4-5), 821–829 (2014).
18. P. Caldas, P. A. S. Jorge, G. Rego, O. Frazão, J. L. Santos, L. A. Ferreira, and F. Araújo, "Fibre Optic Hot-Wire Flowmeter Based on a Metallic Coated Hybrid LPG-FBG Structure," in *Fourth European Workshop on Optical Fibre Sensors* (2010), **7653**, p. 76530B.
19. S. Gao, A. P. Zhang, H.-Y. Tam, L. H. Cho, and C. Lu, "All-optical fiber anemometer based on laser heated fiber Bragg gratings," Opt. Express **19**(11), 10124–10130 (2011).
20. X. Wang, X. Dong, Y. Zhou, Y. Li, J. Cheng, and Z. Chen, "Optical fiber anemometer using silver-coated fiber Bragg grating and bitaper," Sens. Actuators A Phys. **214**, 230–233 (2014).
21. X. Wang, X. Dong, Y. Zhou, K. Ni, J. Cheng, and Z. Chen, "Hot-Wire Anemometer Based on Silver-Coated Fiber Bragg Grating Assisted by No-Core Fiber," IEEE Photon. Technol. Lett. **25**(24), 2458–2461 (2013).
22. Y.-J. Rao, "In-fibre Bragg grating sensors," Meas. Sci. Technol. **8**(4), 355–375 (1997).
23. C. G. Lomas, *Fundamentals of Hot Wire Anemometry* (Cambridge University, 2011).
24. B. D. C. Collis and M. J. Williams, "Two-dimensional convection from heated wires at low Reynolds numbers," J. Fluid Mech. **6**(03), 357–384 (1959).
25. C. Holmes, D. O. Kundys, J. C. Gates, C. B. E. Gawith, and P. G. R. Smith, "150 GHz of thermo-optic tuning in direct UV written silica-on-silicon planar Bragg grating," Electron. Lett. **45**(18), 954 (2009).
26. C. Sima, J. C. Gates, H. L. Rogers, P. L. Mennea, C. Holmes, M. N. Zervas, and P. G. R. Smith, "Ultra-wide detuning planar Bragg grating fabrication technique based on direct UV grating writing with electro-optic phase modulation," Opt. Express **21**(13), 15747–15754 (2013).
27. F. Rafiq, M. Adikan, S. R. Sandoghchi, C. W. Yi, R. E. Simpson, M. A. Mahdi, A. S. Webb, J. C. Gates, and C. Holmes, "Direct UV Written Optical Waveguides in Flexible Glass Flat Fiber Chips," IEEE J. Sel. Top. Quantum Phys. **18**, 1534–1539 (2012).
28. C. Holmes, L. G. Carpenter, J. C. Gates, and P. G. R. Smith, "Miniaturization of Bragg-multiplexed membrane transducers," J. Micromech. Microeng. **22**(2), 025017 (2012).
29. C. Holmes, L. G. Carpenter, H. L. Rogers, J. C. Gates, and P. G. R. Smith, "Quantifying the optical sensitivity of planar Bragg gratings in glass micro-cantilevers to physical deflection," J. Micromech. Microeng. **21**(3), 035014 (2011).
30. T. H. Laby and G. W. C. Kaye, *Tables of Physical and Chemical Constants*, 16th ed. (Longman, 2005).

1. Introduction

Integrating optical fiber with a planar substrate is used throughout photonics. Examples of which include waveguide coupling [1,2], optical pumping [3,4] and fabrication of micromechanical sensor systems [5,6]. Adhesion is usually achieved through use of glues such as epoxy [7], a fusion splice [8] or glass frit [9], which do exhibit limitations. These include poor optical quality, thermal degradation at only a few hundred degrees Celsius, degradation in the presence of common solvents and the potential of introducing micro-damage to the fiber [10]. In this paper we introduce a new method for adhesion that involves the consolidation of glass soot formed through Flame Hydrolysis Deposition (FHD) [11] about a fiber as illustrated in Fig. 1.

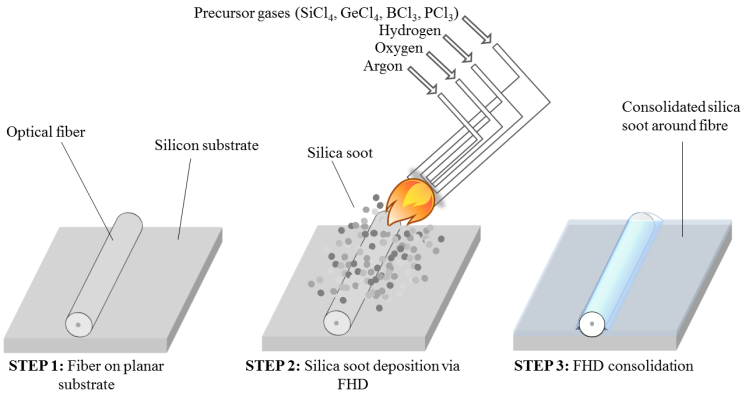

Fig. 1. The three stage process to fabricate a fibre-FHD planar composite.

The resulting glass-fiber composite (SEM imaged in Fig. 2) overcomes the limitations associated with other adhesion methods. Furthermore, it has the added advantage of utilizing

#224955 - $15.00 USD Received 15 Oct 2014; revised 27 Nov 2014; accepted 9 Dec 2014; published 19 Dec 2014

a commercial silica deposition technique that has a low propagation loss [12] and can be doped to manipulate refractive index and stress optic properties [13,14]. The platform is also conducive to planar microfabrication.

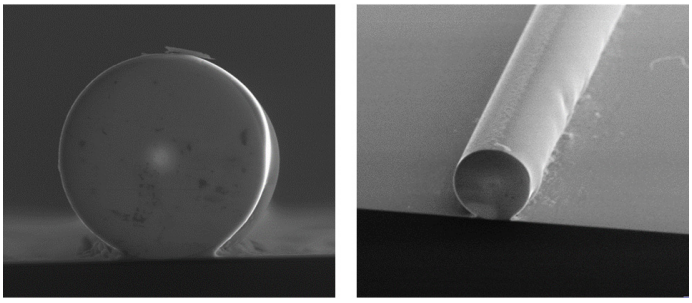

Fig. 2. SEM images of the Fibre-FHD optical composite (FFOC) with an optical fibre diameter of 125µm.

This paper reports the microfabrication of a hot-wire anemometer as a way of demonstrating the capability of the fiber-planar composite.

Micromechanical anemometers have most recently been employed to monitor superfluidic turbulence [15], Karmen vortices [16] and for active flow control in aeronautics [17]. Hot-wire anemometers use an electrically heated wire to monitor fluid velocity. The principle works as fluid flowing past the wire effectively cools the system through forced convection, which typically results in a measureable change in electrical resistance. Similar concepts using hot-wire fiber Bragg gratings (FBGs) have recently been demonstrated [18–21], where the FBGs are directly used to optically monitor thermal fluctuations. However these have not been monolithically integrated. In this work a MOEMS hot-wire anemometer is constructed that uses an exposed section of optical fiber as the 'hot-wire'. The fiber-FHD platform used to realize this is conducive to monolithic microfabrication, enabling micro-heaters to be directly integrated over a selected FBG section.

Concept and theory

The hot-wire anemometer presented in this work consists of a silicon chip on which an optical fiber is adhered using FHD silica. After fabricating the fiber-FHD composite selective etching of silicon and FHD is made to form a bridge of optical fiber 1 mm in length, illustrated in Fig. 3. Selective deposition of gold both onto the exposed fiber and chip is made to form a conducting wire and supply tracks. To monitor thermal fluctuations two FBGs are positioned on the bridge structure (B) and the main body of the chip (A), as illustrated in Fig. 3.

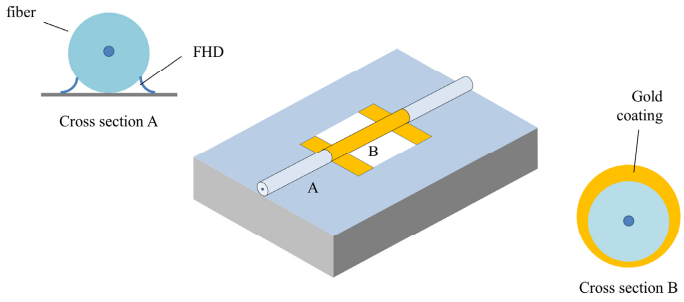

Fig. 3. The geometry of the hotwire anemometer consisting of an optical fibre surrounded by a conducting gold layer. Fibre Bragg gratings are located at A and B. Gold was sputtered resulting in a non-uniform coating around the fibre.

The spectral response of an FBG to physical changes is understood to be [22],

#224955 - $15.00 USD Received 15 Oct 2014; revised 27 Nov 2014; accepted 9 Dec 2014; published 19 Dec 2014

$$\frac{\Delta\lambda_B}{\lambda_0} = (1-\rho_\alpha)\Delta\varepsilon_{axial} + \eta\Delta T \tag{1}$$

where λ_B is the Bragg wavelength, ρ_α is the photoelastic coefficient, ε_{axial} is the strain, η is the thermo-optic constant and T is temperature. For SMF28 the thermo-optic coefficient is approximately 13pm.K^{-1} at 1550nm [22].

The heat transfer of a hot-wire system can be expressed as,

$$\frac{dE}{dt} = W - H \tag{2}$$

where E is thermal energy stored, W is power generated by joule heating and H is heat transferred to surroundings. The heat transfer is the summation of convection, conduction and radiation parts. Considering the steady state condition (dE/dt = 0) and making the assumptions of small radiation and conduction contributions and an equilibrated temperature over sensor length then,

$$I^2R = hA\left(T_w - T_a\right) \tag{3}$$

where I and R are the electrical current and resistance, T_w and T_a are the temperatures of the wire and air respectively, A is the surface area of the wire and h is the heat transfer. Heat transfer is a function of fluid velocity v, which according to King's Law approximates,

$$h = a + bv^c \tag{4}$$

where a, b and c are constants, with the Siddall and Davies corrected empirical value for c being accepted as 0.45 [23]. Combining Eqs. (1-4) the spectral Bragg shift of grating B (see Fig. 3) can be approximated by

$$\Delta\lambda_B = \frac{I^2R\lambda_0\eta}{A(a+bv^{0.45})} \tag{5}$$

This equation is valid only when King's Law sufficiently approximates heat transfer.

Considering Reynolds number R_e as a descriptor for characteristic fluidic phenomena. For a hotwire anemometer the Reynolds number is,

$$R_e = \frac{vd}{\gamma} \tag{6}$$

where v is the perpendicular fluid velocity, d is the diameter of the cylinder and γ is the kinematic viscosity. Rigorous description of hotwire anemometers at very low Reynolds numbers are understood to exhibit a so called 'buoyancy effect', where free convection dominates over forced convection. One such phenomena described by Collis and Williams [24] highlighted that free convection is significant when the Reynolds number is less than the cube root of the Grashof number G_r shown in following equation,

$$R_e > G_r^{1/3} \tag{7}$$

The following results shall show the fabricated device approximating King's Law and at low fluid velocity deviating from this trend and exhibiting molecular free convection phenomena.

Results

The fabricated device consisted of bridge section that was 1 mm in length and contained a Bragg grating of equal length. Additionally a Bragg grating was defined away from bridge structure to monitor thermal fluctuations for the bulk chip. Both Bragg gratings were

#224955 - $15.00 USD Received 15 Oct 2014; revised 27 Nov 2014; accepted 9 Dec 2014; published 19 Dec 2014

fabricated using direct UV writing (DUW) after the fiber was bound to the wafer [25–27] using FHD.

FHD silica soot was formed through burning precursors of $SiCl_4$, PCl_3 and BCl_3 at flow rates of 139, 31 and 70 sccm respectively, using the torch configuration illustrated in Fig. 1. The oxyhydrogen flame produced by the torch had O_2, H_2 and Ar flow rates set to 6.5, 1.9 and 8.0 $l.min^{-1}$ respectively. Consolidation of the soot was subsequently made at 1260°C, after which thickness and refractive index were measured using a Metricon Prism Coupler, giving values of 2μm and 1.4452 respectively.

The micro-mechanical bridge structure was defined through the selective removal of silicon and FHD silica substrate beneath the adhered fiber, using standard planar processing techniques [28,29]. The bridge was subsequently patterned with gold through forming a mask and depositing gold through sputtering. Two gold contacts at the roots of the bridge were also defined to assist electrical connection. The resistance of the sampled element was 0.16 kΩ.

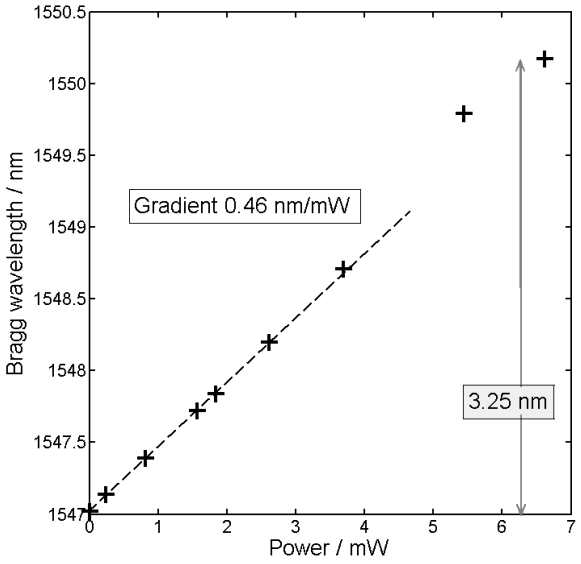

Fig. 4. Spectral tunability with respect to operational power.

Figure 4 illustrates the spectral tuning of grating B (see Fig. 3) with supplied electrical power, demonstrating an efficiency of 0.46 nm/mW, which is more efficient than comparable optically heated FBG anemometers [18–21]. The spectral response is linear with increasing power except for higher operational powers, where the spectrum becomes characteristically chirped shown in Fig. 5. It is suggested that the cause of chirp is a consequence of heat dissipation through the roots of the bridge resulting in a temperature variation over the grating.

The thermo-optic coefficients of the two gratings were calibrated by placing the chip in an oven over a 20-60°C temperature range. The measured values were 14.0 ± 0.4 $pm.K^{-1}$ in the body of the chip (position A in Fig. 3) and 14.1 ± 0.4 $pm.K^{-1}$ in the hot-wire section (position B). This is comparable to the accepted FBG response of 13$pm.K^{-1}$ at 1550nm, with the small increase being a likely result of the silicon substrate having a greater thermal expansion coefficient than the silica fiber.

#224955 - $15.00 USD Received 15 Oct 2014; revised 27 Nov 2014; accepted 9 Dec 2014; published 19 Dec 2014

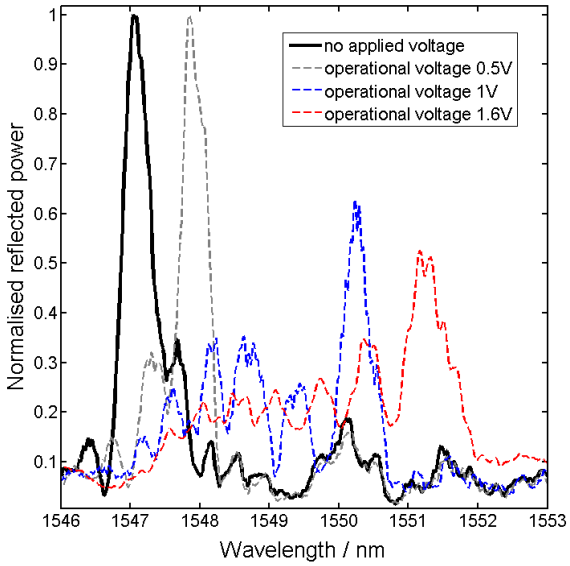

Fig. 5. Spectral tunability for selected operational voltages, indicating presence of spectral chirp.

It is observed in Fig. 5 that a 1.6 V (16mW) operational voltage corresponds to ~4.1 nm of Bragg grating shift. Inferring spectral shift as thermo-optic response, this is equivalent to an operational temperature of 584 ± 8 K, notably a temperature that exceeds the operational specification of most glues.

The following data considers a maximum 1V applied operational voltage (corresponding to 6.25mW). The spectral shift of grating B at this drive voltage is 3.23nm, from which an inferred operational temperature of 522 ± 6 K is assumed. This is approximately 100 K greater than that achieved with optically heated FBG approaches [18–21] and more typical of traditional hot-wire anemometers [23].

The following experimental data was taken using dry nitrogen gas, which shall be termed as 'fluid' in the following discussion. Fluid velocity was calibrated using a commercial hotwire TSI Airflow anemometer (TA460 with the Probe 484). The specified error of the commercial anemometer is ± 15 $mm.s^{-1}$ or ± 3% whichever is greatest. The gauge and chip were located within a cylindrical tube such that they were level and perpendicular to the flow.

Figure 6 depicts data taken at a 6.25 mW operational power. It is noted that two distinct regimes are observed from the data. There is a high fluid velocity regime >10 $mm.s^{-1}$, where the data follows King's Law as understood in Eq. (5) and a lower fluid velocity regime <10 $mm.s^{-1}$, where the data deviates from King's Law.

The deviation from King's Law occurs at ~11 $mm.s^{-1}$, which from Eq. (6) corresponds to a Reynolds number of 0.13 (considering a fiber diameter of 125µm and a kinematic viscosity of 0.014 [30]). Through extrapolating the work by Collis and Williams [24] this is the expected value at which the interaction between forced and free convection becomes significant, termed as buoyancy effects.

#224955 - $15.00 USD Received 15 Oct 2014; revised 27 Nov 2014; accepted 9 Dec 2014; published 19 Dec 2014

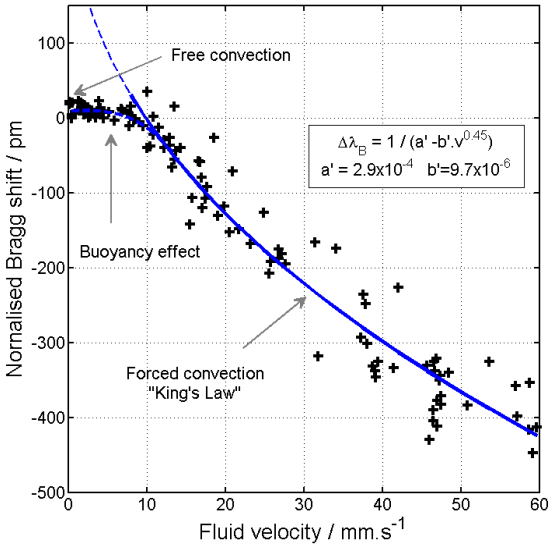

Fig. 6. The spectral response of a Bragg grating located in a hot-wire element (1V operating potential) subject to increasing air-velocity.

Greatest sensitivity occurs at lower air velocities that still approximate King's Law. Taking a fluid velocity of 15mm.s^{-1} a corresponding 12.3 pm/mm.s^{-1} sensitivity can be inferred. To quantify resolution a constant fluid flow was established at this fluid velocity and a 5-sample standard error of 2 pm was measured. This suggests a maximum resolvable air velocity of ~0.2 mm.s^{-1} for this operational voltage. This measurement removed the error most notable in Fig. 6 that is associated with the commercial hot-wire anemometer used for calibration (± 15 mm.s^{-1}). The result shows greater sensitivity than optically heated FBGs [18–21], which typically show 10's mm.s^{-1} resolution. This difference is believed to be a result of the greater operational temperatures that are achievable with the reported device.

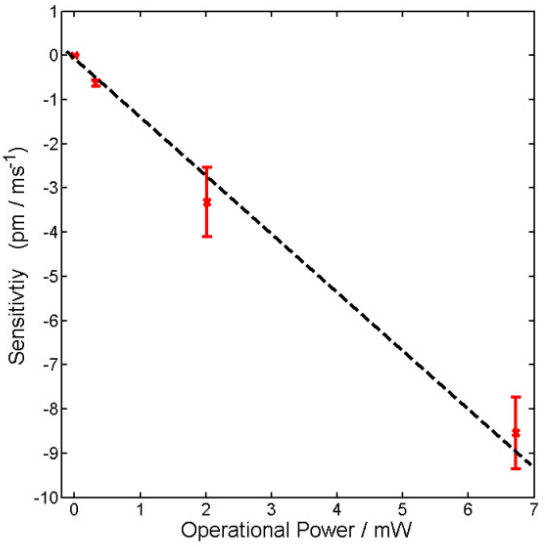

Fig. 7. Device sensitivity for a Bragg grating anemometer, with respect to operational voltage.

#224955 - $15.00 USD Received 15 Oct 2014; revised 27 Nov 2014; accepted 9 Dec 2014; published 19 Dec 2014

Figure 7 illustrates the sensitivity and associated error at mid-range test velocity (i.e. sensitivity at 30 $mm.s^{-1}$) for several operating powers. As expected from Eq. (5) sensitivity follows linearly with operational power (I^2R), with larger operational powers having greater sensitivity.

It must be noted that there was a relatively small spectral increase in Bragg grating 'A', during measurements. This corresponded to 3.6 K at maximum operational power and is a result of bulk heating. One additional use for this could be monitoring of the drive current.

Conclusions

We have demonstrated for the first time a fiber-FHD composite. The application chosen for demonstration has been a hot wire anemometer. It was shown that the composite has the ability to withstand planar processing and inferred operational temperatures exceeding 580K. Furthermore, Bragg gratings can be directly written into the structure to measure physical actuation.

The fabricated device had a maximum resolvable air velocity of 0.2 $mm.s^{-1}$ and was sufficiently sensitive at low velocities to measure fluidic buoyancy effects, when free convection becomes significant over forced convection.

#224955 - $15.00 USD Received 15 Oct 2014; revised 27 Nov 2014; accepted 9 Dec 2014; published 19 Dec 2014